

Study on synthesis and adsorption properties of ReO_4^- ion imprinted polymer

Xiaoyan Zhang^{1,2} · Weiwei Jia^{1,2} · Donghao Li³ · Chunli Liu^{1,2} · Runtian Wang^{1,2} · Ke Li^{1,2} · Hui Li^{1,2} · Zhenbin Chen^{1,2} · Yuan Sun⁴ · Juan M. Ruso⁵ · Dongdong Hu⁶ · Zhen Liu⁷ 

¹State Key Laboratory of Advanced Processing and Recycling of Nonferrous Metals, Lanzhou University of Technology, Lanzhou 730050, Gansu, China.

²School of Material Science and Engineering, Lanzhou University of Technology, Lanzhou 730050, Gansu, China

³College of Materials Science and Engineering, Nanjing Tech University, Nanjing 211816, Jiangsu, China

⁴Institute of Metal Research, Chinese Academy of Sciences, Shenyang 110016, Liaoning, China

⁵Soft Matter and Molecular Biophysics Group, Department of Applied Physics, University of Santiago de Compostela, 15782 Santiago de Compostela, Spain

⁶State Key Laboratory of Chemical Engineering, East China University of Science and Technology, Shanghai, China

⁷Department of Physics and Engineering, Frostburg State University, Frostburg, MD 21532, USA

Abstract

Water solution polymerization was adopted to prepare perrhenate ion imprinted polymers in this work, and preparation conditions, such as molar ratio of acrylic acid, N,N - methylene double acrylamide, hydrogen peroxide and ascorbic acid to N-vinyl pyrrolidone, polymerization time and temperature on adsorption separation property were investigated and optimized using adsorption quantities and separation degree as indexes. To enhance the adsorption selectivity, adsorption properties of samples prepared under different conditions were conducted in a mixture aqueous solution of ammonium perrhenate and potassium permanganate with the molar ratio of 1:1. Results showed that as the molar ratio of N,N - methylene double acrylamide, acrylic acid, hydrogen peroxide, ascorbic acid to N-vinyl pyrrolidone were 2.0, 1.9, 0.03, and 0.003 respectively, the reaction temperature and time were 35 °C and 24 h, adsorption quantities and separation degree arrived at 0.037 mmol/g and 2.31, respectively, while the adsorption capacities and separation degree of non-imprinted polymers were only 0.009 mmol/g and 0.22. Besides, study was also discovered that the prepared samples presented an exciting reusable stability. Based on samples prepared under optimal conditions, the structure was characterized by Fourier transform infrared spectroscopy, scanning electron microscope, transmission electron microscope, BET surface area and thermogravimetric analysis using non-imprinted polymer prepared under the same conditions as a control. Finally, the adsorption thermodynamics and kinetics were studied, and the kinetics documented that the adsorption of perrhenate ion imprinted polymers was a zero-order model process. The thermodynamics presented the adsorption was more suitable to be expressed by Langmuir model, and Scatchard analysis revealed that heterogeneous binding sites were formed in IIP.

Keywords Ion imprinted polymers · Ammonium perrhenate · Water solution polymerization · Adsorption

Introduction

Superalloy has been widely used in fields of defense, aerospace, nuclear energy, electronics [1, 2], etc. To meet the demand of excellent strength and flexibility at temperature higher than 1500 °C, superalloy is always fabricated by adding some super temperature resistant elements, such as Cr, Ru, Re, W and Ta et al, to the matrix of Fe, Co, and Ni. According to reports, Re was the most important alloy element of superalloy because it can elevate the temperature resistance of superalloy effectively [3, 4], and that the content of Re in superalloy [5] increased continuously to meet the increasingly stringent requirements. Thus, Re is demanded urgently. However, the reserves of Re are inadequate related to the increasing demand, as less than 2500 tons of Re have been found all over the world [6], and what's more, the content of Re in mineral is very small as the maximum content in the ore shall not exceed 0.3%. According to reports, most of Re is always associated in the molybdenite [7] and redruthite, and which, naturally, dramatically increase the difficulty of purification [8]. Added to the serious demand of high purity in application (about 99.999%), Re obtained from general metallurgical engineering can be applied hardly. Whereas, further purification using conventional approach would need larger cost but cannot ensure the purity meeting the demand. Thus, Re existed in above minerals is always abandoned, which further enlarge the imbalance between supply and demand. Therefore, it is of great significance to develop a novel material that can separate Re targeted from the complex environment to improve the purity [9–11]. If the material had been developed, the aim that full utilization of mineral resources would be realized, and the problem of supplement insufficient of Re would also be alleviated.

A stable and a segregative state would be benefit for materials and technics design and development. The general exist form of Re in the metallurgical is ReO_4^- [12], so it should be important to prepare a material that could target to ReO_4^- in solution that containing many components. Ion imprinting polymer (IIP) was a novel type of material which has been developed from molecular imprinting technology [13, 14]. Because of the simple preparation process and the excellent specific selectivity [15–17], IIP has developed rapidly and been used widely in many fields, for example, membrane separation [18–20], sensors [21–23], wastewater treatment [24–27], determination of trace ions [28–32], solid phase extraction [33–38], high performance liquid chromatography [39] and drug delivery [40, 41] among others. It has become one of the most representative advanced affinity adsorption separation material [42, 43]. At present, obstacles for the application of IIP are the selectivity and reusability. To improve the selectivity, IIP was always prepared in non-aqueous media [44] to ensure the sufficient self-assembly among template ions and monomers, which could not ensure the selectivity

and reusability in actual application because the terminal application environment of IIP was aqueous solution [45, 46]. Due to the interaction differences between solvent and IIP, especially the variation of hydrogen bond energy, the matrix structure of IIP prepared in non-aqueous media could not preserve well naturally, let alone imprinted cavities. Thus, the weakened selectivity and reusability would be inevitably. So how to prepare IIP in aqueous media with good selectivity and reusability is still an important problem [47, 48].

Based on our previous study in MIP [49, 50], this work prepared a ReO_4^- -IIP in aqueous media by solution polymerization. During this process, ammonium perrhenate was adopted as template, N-vinyl pyrrolidone (NVP) and acrylic acid (AA) was selected as functional monomer, N, N - methylene double acrylamide (NMBA) was used as crosslinker, hydrogen peroxide (H_2O_2)-ascorbic acid (Vc) was chosen as initiator, and water was specially conscripted as solvent. To ensure the selectivity and reusability of perrhenate ion imprinted polymers (ReO_4^- -IIP), permanganate ion (MnO_4^-), which possesses the same spatial structure and similar interatomic interaction as ReO_4^- , but the molecular size was smaller, was selected as interference to optimize the special selectivity of ReO_4^- -IIP using adsorption quantities (Q) and separation degree (R) as the focused parameters. After each condition was investigated in detail, ReO_4^- -IIP was prepared under optimal conditions. Experiment result documented ReO_4^- -IIP prepared under optimal conditions presented a high specific recognition of ReO_4^- from a mixture of NH_4ReO_4 and KMnO_4 , NH_4ReO_4 and with $(\text{NH}_4)_2\text{MoO}_4$, NH_4ReO_4 and NH_4VO_3 , and NH_4ReO_4 and NiCl_2 with equimolar concentration. Besides, ReO_4^- -IIP also presented the excellent reusability. Based on ReO_4^- -IIP prepared under optimal conditions, the structure was characterized by Fourier transform infrared spectroscopy (FTIR), scanning electron microscope (SEM), Transmission electron microscope (TEM), BET surface area and thermogravimetric analysis (TGA) using non-ion imprinted molecular polymer (NIIP) as control. Finally, adsorption kinetics and adsorption thermodynamics were studied.

Experimental

Material

Acrylic acid (AA CP), Polyvinyl alcohol (1788) and Na_2HPO_4 (AR) were purchased from Tianjin Guangfu Fine Chemical Research Institute. N-vinylpyrrolidone (NVP, CP) was presented by Henan Luoyang Boai New Open Source Co., Ltd.. N, N-methylenebisacrylamide (NMBA, CP) was purchased from Tianjin Komio Reagent Co., Ltd.. Ascorbic acid (Vc, AR) was presented by Tianjin Deen Chemical Reagent Co., Ltd.. 30% H_2O_2 (AR) and citric acid (CA, AR)

was purchased from Tianjin Hengxing Chemical Reagent Co., Ltd.. Ethanol were analysis grade and was provided by Yantai Shuangshuang Chemical Co., Ltd.. Ammonium perhenate (99.9999%) was purchased from Hunan Chuangrun Mineral Resources Co., Ltd.. Potassium permanganate was analytical grade and was presented by Chongqing Changyuan Chemical Group Co., Ltd.. Ethyl violet (90%) was presented by Shanghai Hongyi Electronics Co., Ltd.. Distilled water was prepared in our lab. All compounds were used without any treatment expect for that special introduced.

Determination of maximum adsorption wavelengths

The maximum absorbance wavelengths of ReO_4^- and MnO_4^- were investigated with a 752 N spectrophotometer (Shanghai Precision and Scientific Instrument Co. Ltd., Shanghai, China) by the full wavelength scanning method. Both ethyl violet photometry [51] and direct measurement were investigated to measure the maximum absorbance wavelength of ReO_4^- and MnO_4^- respectively, and results were shown in Fig. S1(a) and (b) in supplement materials.

Relationship between absorbency and concentration

The relationship between absorbency and concentration of NH_4ReO_4 and KMnO_4 in the range of (0.19, 0.93 mmol/L) in ethyl violet chromatography method were measured at 658 nm, KMnO_4 in the range of (0.19, 0.93 mmol/L) in direct determination method was measured at 500 nm, then plots were regressed, and results were shown in Fig. S2(a) and (b).

Synthesis of ReO_4^- -IIP

First, 25 mL distilled water and 18.715 mmol NVP were added into a three-necked flask equipped with a gas inlet and outlet tube, a constant pressure funnel and a thermometer. Then, NMBA with $n(\text{NMBA})/n(\text{NVP}) = 2.08$ was added. After NMBA dissolved completely, NH_4ReO_4 and AA with $n(\text{NH}_4\text{ReO}_4)/n(\text{NVP}) = 0.03$ and $n(\text{AA})/n(\text{NVP}) = 1.95$ were added into. Sealed the flask and fixed it on a magnetic stirrer. After agitating for 10 min, nitrogen (N_2) was purged to the flask for 10 min. Then, H_2O_2 and Vc solutions with $n(\text{H}_2\text{O}_2)/n(\text{NVP}) = 0.03$ and $n(\text{Vc})/n(\text{NVP}) = 0.003$ were added to the flask. After the magnet in the flask could not rotate, the flask was immersed into a 35 °C constant temperature water bath for 24 h. After that, polymer in the flask was taken out and cut into small pieces and placed into a 90 °C oven for 24 h. After polymer pieces dried, they were smashed. Samples with size of 50–150 mesh were collected and placed into a 200 mesh tea bag. Placing the bag into a Soxhlet extractor and resining with 95% alcohol till the adsorption of alcohol solution became a constant. Finally, samples were dried at 90 °C to constant and stored in desiccators for further use. As references, ReO_4^- -

NIIP were prepared following the same procedure except template was not introduced.

Characterizations of ReO_4^- -IIP and ReO_4^- -NIIP

ReO_4^- -IIP and ReO_4^- -NIIP were ground into powder, and then FTIR characterization was conducted on a Nicolet Nexus 670 using (American Nicolet Corporation, Madison, Wisconsin, USA) using potassium bromide pressed-disk technique, respectively. The scan range was 4000 to 400 cm^{-1} .

After the template ion, ReO_4^- , was extracted completely, some samples were freeze-dried for to constant weight. Thereafter, the morphology was characterized by TEM (JSM-6701F, Japan) and SEM (TECNAI G² TF20, USA).

Nitrogen sorption analysis was carried out on about 0.2 g sample of IIP and NIIP by surface area and porosity analyzer (ASAP 2020). The samples were degassed for 9 h at -197.286 °C. The surface area of the imprinted polymers was derived from the adsorption isotherms using a BET method.

The thermal stability of leached- ReO_4^- -IIP and unleached- ReO_4^- -IIP samples were performed at a thermogravimetric analysis (TGA) by synchronous thermal analyzer (STA449C, Germany).

Determination of adsorption kinetics

0.1000 g of samples were placed into a 200 mesh tea bag (7.6 × 50 mm), and then the tea bag was sealed and placed in a beaker which was contained 50.00 mL of 0.75 mmol/L NH_4ReO_4 solution and had been constant to 30 °C, after adsorption for given time, the tea bag was removed, and the absorbency of the raffinate was tested with a UV-visible spectrophotometer at $\lambda = 658$ nm using ethyl violet photometry. The adsorption quantities (Q) of ReO_4^- -IIP was calculated according to eq. (1)

$$Q = \frac{\delta C_0 - C_t \times V}{W} \quad (1)$$

Where, Q was the adsorption quantities of the ReO_4^- -IIP (mmol/g), C_0 represented the concentration of NH_4ReO_4 in the initial solution (mmol/L), C_t was the concentration of NH_4ReO_4 in the solution after adsorption for time t (mmol/L), V stood for the volume of the adsorption solution (L) and W was the mass of ReO_4^- -IIP (g).

Determination of adsorption thermodynamics

10 parts of 0.1000 g ReO_4^- -IIP were placed into a series of 200 mesh tea bag (7.6 × 50 mm) labeled with 1–10, and then above tea bag were loaded into ten flasks which had been loaded with 30.00 mL of NH_4ReO_4 solution with

concentration range from 0.25 to 2.5 mmol/L and had been constant to 30 °C, respectively. As adsorption arrived at equilibrium, the absorbance of the raffinate was tested with an UV-visible spectrophotometer at $\lambda = 658$ nm using ethyl violet photometry method. Q_e was calculated with eq. (2).

$$Q_e = \frac{C_0 - C_e}{W} \times V \quad (2)$$

Where, Q_e was the equilibrium adsorption quantities of the ReO_4^- -IIP (mmol/g), C_e was the concentration of NH_4ReO_4 in the solution after adsorption arrived at equilibrium time (mmol/L).

Determination of adsorption capacity

0.2000 g of ReO_4^- -IIP were placed into a 200 mesh tea bag (7.6×50 mm), and then the tea bag was loaded into a 50 mL beaker which contained 30.00 mL of mixed solution of NH_4ReO_4 and KMnO_4 (The concentration of each component before mixing was 0.75 mmol/L) and had been constant to 30 °C. After adsorption to equilibrium, the tea bag was removed, and the solution was stood for 15 min, the absorbance of the raffinate was measured at 658 nm using ethyl violet photometry methods and at 500 nm directly, respectively. After the concentration of ReO_4^- and MnO_4^- in raffinate was calculated, the adsorption capacities of ReO_4^- -IIP for ReO_4^- and MnO_4^- were calculated according to the eqs. (3)-(4).

$$Q_{\text{ReO}_4^-} = \frac{(C_0(\text{ReO}_4^-) - C(\text{ReO}_4^-)) \times V}{W} \quad (3)$$

$$Q_{\text{MnO}_4^-} = \frac{(C_0(\text{MnO}_4^-) - C(\text{MnO}_4^-)) \times V}{W} \quad (4)$$

Where, $Q(\text{ReO}_4^-)$ and $Q(\text{MnO}_4^-)$ were the equilibrium adsorption capacities of ReO_4^- and MnO_4^- (mmol/g), respectively, $C_0(\text{ReO}_4^-)$ and $C_0(\text{MnO}_4^-)$ were the concentration of ReO_4^- and MnO_4^- in the initial solution (mmol/L), $C(\text{ReO}_4^-)$ and $C(\text{MnO}_4^-)$ stood for the concentration of ReO_4^- and MnO_4^- in the raffinate after adsorption to equilibrium (mmol/L), V was the volume of the adsorption solution (L).

To investigate the effects of reaction temperature, time and the molar ratios of NMBA, AA, H_2O_2 , Vc to NVP on the adsorption capacity of ReO_4^- -IIP. The variables under different conditions were studied by the control variable method.

Calculation of separation degree

After $Q(\text{ReO}_4^-)$ and $Q(\text{MnO}_4^-)$ were measured, the separation degree (R) of $\text{ReO}_4^-/\text{MnO}_4^-$ could be calculated according to the eq. (5).

$$R = \frac{Q(\text{ReO}_4^-)}{Q(\text{MnO}_4^-)} \quad (5)$$

Results and discussion

Establishment of the concentration measuring method

To optimize the selectivity of ReO_4^- -IIP effectively, MnO_4^- was conscripted as the interference. The reason why MnO_4^- was selected as the interference contained following reasons: 1) The spatial structure. Both the structure of ReO_4^- and MnO_4^- were shown in Fig. S3, it could be found MnO_4^- was similar with ReO_4^- . 2) Both were bonded with O, which meant the hydrogen bond energy was similar. 3) The molecular size of MnO_4^- was smaller than ReO_4^- . Just for above reason, MnO_4^- could easily enter the imprinted cavities of ReO_4^- , thus, if ReO_4^- -IIP exhibited excellent separation performance in the mixture of MnO_4^- and ReO_4^- , IIP would be ensured to possess the excellent selectivity to ReO_4^- in any other complex environment.

In this experiment, the adsorption solution was an equimolar concentration mixed solution of ReO_4^- and MnO_4^- . To ensure the accuracy of results, the relationship between absorbance and wavelength was investigated, and results were shown in Fig. S1(a). It could be found that the maximum absorbance wavelength of ReO_4^- and MnO_4^- with ethyl violet photometry was 658 nm and 432 nm, respectively, but at the maximum absorbance wavelength of ReO_4^- , MnO_4^- also showed certain absorbency, and similar result was also occurred for that of MnO_4^- . Thus, the concentration determination accuracy for both ReO_4^- and MnO_4^- would be influenced, and which further result in large error or even mistake for Q and R . To resolve this problem, the adsorption of ReO_4^- and MnO_4^- was investigated directly, and results were shown in Fig. S1(b). It presented when ethyl violet was not introduced, ReO_4^- would not show adsorption at the maximum absorbance wavelength of MnO_4^- , which meant the concentration of MnO_4^- could be determined directly first, and then ReO_4^- would be calculated if there was no influence between ReO_4^- and MnO_4^- and the concentration of ReO_4^- and MnO_4^- was fell in the linear range.

Fig. S2 (a) showed the relationship between absorbency and concentration of NH_4ReO_4 and KMnO_4 at 658 nm. It presented a well linear relationship for both NH_4ReO_4 and KMnO_4 in the concentration range of 0.19–0.93 mmol/L, which meant concentration of NH_4ReO_4 could be obtained accurately if there was no interaction between ReO_4^- and MnO_4^- , and if the concentration of MnO_4^- could be determined accurately.

Because ReO_4^- was undisturbed with the determination of MnO_4^- at 500 nm in direct measurement, the concentration of MnO_4^- could be determined if a well linear relationship between absorbency and concentration of KMnO_4 at the ranged of 0.19–0.93 mmol/L could be obtained. Fig. S2 (b) documented the concentration of KMnO_4 could be obtained accurately.

To further investigation whether there was interaction between ReO_4^- and MnO_4^- , the relationship between absorbency and molar ratio of NH_4ReO_4 and KMnO_4 in mixture keeping the total concentration as 0.93 mmol/L was explored. Figure 1 presented in the molar ration rang of $\text{NH}_4\text{ReO}_4/\text{KMnO}_4 = 4/6-8/2$, a well linear relationship was displayed, which illustrated there was no interaction between ReO_4^- and MnO_4^- . What's more, the absorbency of mixture was equal to the addition of pure ReO_4^- and MnO_4^- solution with the same concentration as them in mixture, which documented there was not any interaction between ReO_4^- and MnO_4^- , and ensured the determination of the concentration of ReO_4^- could be carried out undoubtedly. According to above work, we concluded the concentration of ReO_4^- could be calculated with following process:

Firstly, the absorbance of MnO_4^- at 500 nm was calculated by eq. (6):

$$A_{\text{MnO}_4^-} = 0.19353C_{\text{MnO}_4^-} - 0.05767 \quad (6)$$

then, the absorbance of ReO_4^- at 658 could calculated by eq. (7):

$$A_{\text{ReO}_4^-} = A - A_{\text{MnO}_4^-} \quad (7)$$

Finally, the concentration of ReO_4^- could be calculated by eq. (8):

$$A_{\text{ReO}_4^-} = 1.90302C_{\text{ReO}_4^-} - 0.30411 \quad (8)$$

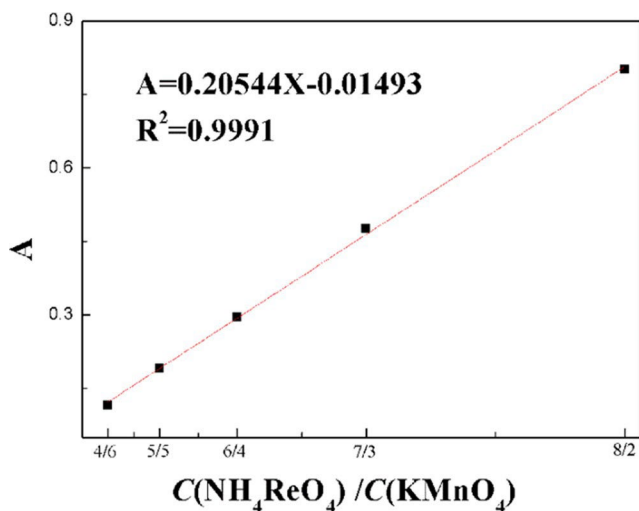


Fig. 1 The relationship between the absorbency and molar ratio (A) of $\text{NH}_4\text{ReO}_4/\text{KMnO}_4$

Characterizations of ReO_4^- -IIP and ReO_4^- -NIIP

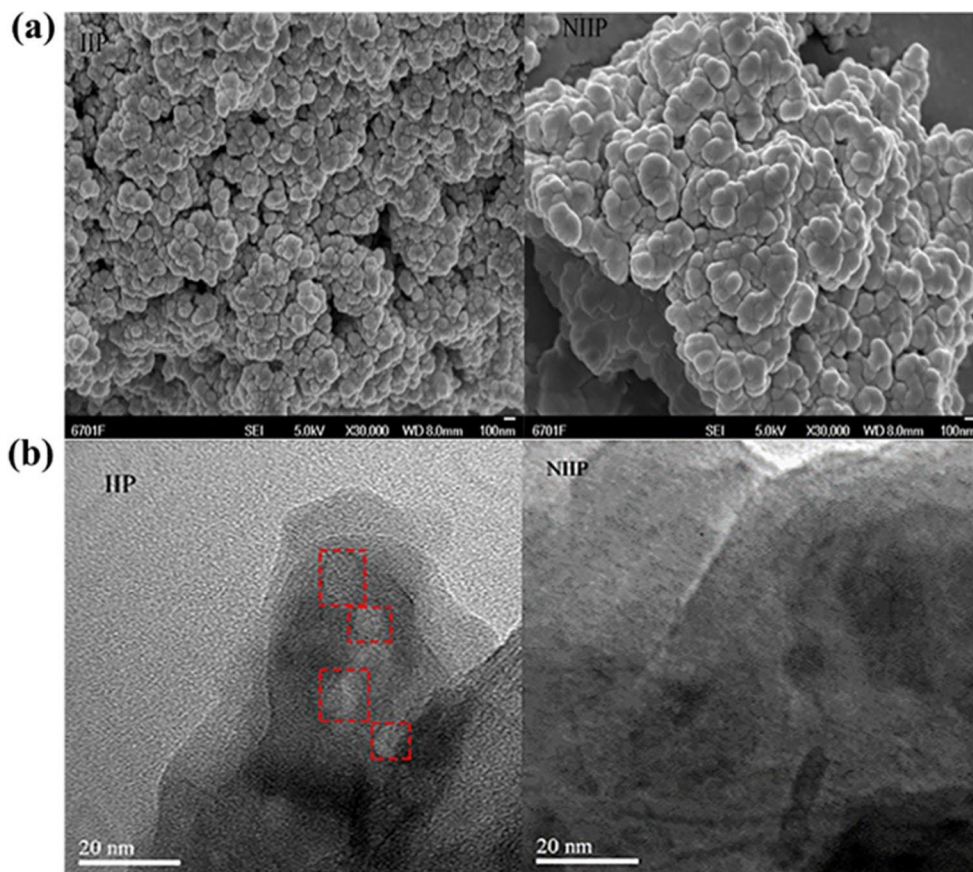
Figure 2 presented FT-IR spectra of ReO_4^- -IIP (leached and un-leached) and ReO_4^- -NIIP (samples were dried to constant weight in 80 °C vacuum oven), the characteristic absorption peaks of leached and un-leached were basically same, which proved that they belong to the same kind of polymer. However, if compare three FT-IR spectrum in detail, the differences between them could be found as follows: for leached

and un-leached, peaks at 3415 cm^{-1} , 1718 cm^{-1} , 1386 cm^{-1} and 1222 cm^{-1} red shift to 3340 cm^{-1} , 1714 cm^{-1} , 1382 cm^{-1} and 1216 cm^{-1} , and peaks at 2940 cm^{-1} , 1646 cm^{-1} , 1527 cm^{-1} and 1446 cm^{-1} blue shift to 2942 cm^{-1} , 1658 cm^{-1} , 1535 cm^{-1} and 1459 cm^{-1} , and the characteristic peaks at 3415 cm^{-1} (O-H), 1658 cm^{-1} (C=O), and 1535 cm^{-1} (N-H, C=C) were significantly enhanced, which was mainly due to the formation of self-assemble structure between the template ion ReO_4^- and the functional monomer, so that the peak intensity of the corresponding characteristic peak was significantly improved, thereby making the peak intensity of the corresponding characteristic peak [52, 53]. For leached and NIIP, peaks at 3340 cm^{-1} , 2942 cm^{-1} , 1535 cm^{-1} and 1112 cm^{-1} blue shift to 3357 cm^{-1} , 2960 cm^{-1} , 1542 cm^{-1} and 1124 cm^{-1} , and peaks at 1658 cm^{-1} , 1459 cm^{-1} and 1216 cm^{-1} red shift to 1650 cm^{-1} , 1450 cm^{-1} and 1211 cm^{-1} . Above difference implied the assembly among ReO_4^- , AA and NVP resulted in the difference between ReO_4^- -IIP and ReO_4^- -NIIP in aggregation structure. What's more, a peak at 804 cm^{-1} of the stretch vibration of Re-O in un-leached sample was not observed in leached and NIIP, which presented the smaller difference in structure between them, and meant after leaching, the structure of IIP could change in a small degree, which might be the basic reason of IIP could not be applied with a complete stable property.

However, FT-IR could not give an obvious distinction between ReO_4^- -IIP and ReO_4^- -NIIP in aggregation structure.

To achieve this aim, TEM and SEM were adopted to find the difference between surface morphology of IIP and NIIP to further characterize the structural differences. Figure 3 (a) and (b) of SEM and TEM documented ReO_4^- -IIP was different obviously from NIIP in surface morphology. SEM results showed that ReO_4^- -IIP formed imprinted cavities, while NIIP has no obvious cavities and was densely arranged. In the TEM (The marked parts were the imprinted cavities of the ReO_4^- -IIP, since H_2O was taken part in the coordination with ReO_4^- , the size of the imprinted cavities was larger than that of the theoretically calculated value from ReO_4^- model), IIP presented regular imprinted cavities at the fracture surface, the shape of cavities were evenly arranged, and the structure of polymer matrix was incompact, while no similar shape cavities were observed in NIIP and the structure of polymer matrix was compact. The results indicated that IIP formed imprinted cavities.

Fig. 2 SEM (a) and TEM (b) of ReO_4^- -IIP and NIIP



To evaluate the structure difference of IIP and NIIP at the macro level, BET was also adopted. The nitrogen adsorption-desorption isotherms of IIP and NIIP microspheres were displayed in Fig. 4 (a) and (b), which could be classified as Type IV with H3 hysteresis loops according to the type of adsorption isotherm, indicating that imprinted polymer possess mesoporous structure [54]. Table 1 shows the pore size

distribution (such as total pore volume (V_p), average pore width (d_p) and surface area (S_{BET}) calculated by BJH and BET method from the adsorption isotherms, respectively. It could be seen BET surface area of IIP and NIIP were 129.6934 and 98.8012 m^2/g , and d_p of IIP and NIIP are 17.2639 nm and 11.37749 nm, respectively. Compared with IIP, the physical characteristic parameters of NIIP was significantly reduced, which could be ascribed to the pores constriction and pores collapse mainly sourced from the high hydrophilic interaction of functional groups in polymer [49, 50].

Figure 5 was the TGA curves of IIPs with leached and un-leached. It could be found that both leached and un-leached IIP presented three stages of thermal weightlessness, as Table 2 showed. The first stage of thermal weight loss was the solvent molecules, free water and bound water in sample [55, 56]. The second stage of thermal weight loss was the dehydration and decarboxylation between polymer molecular chains and within the molecule to form anhydride [57, 58]. The third stage of thermal weight loss was polymer chain breakage and degradation. In addition, the thermal loss of samples 1 and 2 were very similarly in three stages, and the degradation was completed before 550 $^{\circ}\text{C}$. However, the thermal degradation degree of un-leached was obviously higher than that of leached, which could be ascribed to the existence of Re in samples mainly. Because ReO_4^- could decompose to

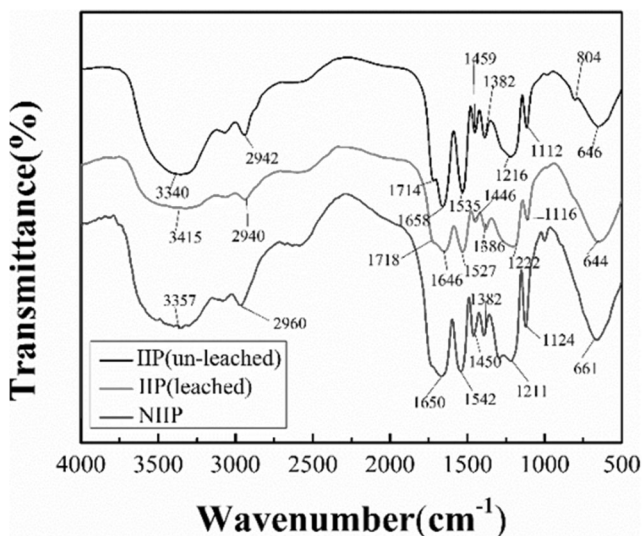


Fig. 3 FTIR spectra of IIP (leached and un-leached) and NIIP

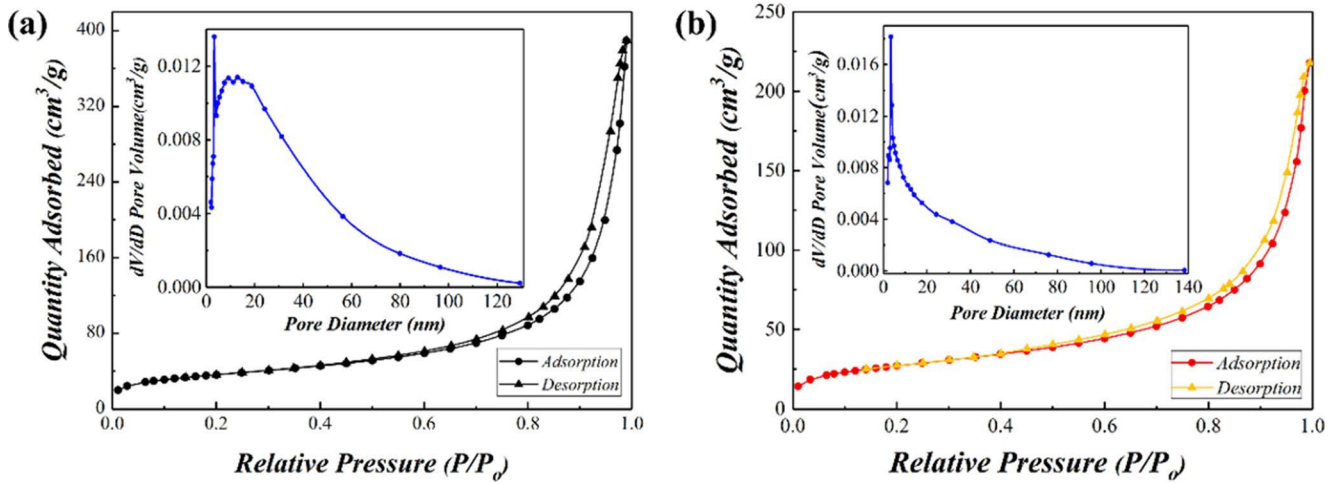


Fig. 4 The nitrogen adsorption-desorption isotherms of IIP and NIIP microspheres

difficult volatilization product, such as ReO_4 , Re_2O_7 , ReO_3 , ReO_2 and Re et al., as temperature was higher than 400°C [59], the remained mass of it after complete degradation was higher could be understood easily.

Adsorption kinetics of ReO_4^- -IIP

The relationship between adsorption capacity (Q_t) and adsorption time (t) was shown in Fig. S4 Q_t increased with prolong of t monotonously till the adsorption equilibrium was arrived after 240 min. A large number of imprinting cavities needed template ions to decrease the surplus bonding energy vigorously, the adsorption of ReO_4^- into the imprinted cavities could be understood easily, and the monotonous increase of Q_t with t till it kept as a constant naturally. Due to the steric resistance of IIP matrix, ReO_4^- solution needed time to diffuse through the matrix layer-by-layer gradually, and the adsorption took place with layer-by-layer way relatively, so the adsorption needs longer time to arrive at its equilibrium.

To further investigate the kinetics of the adsorption process, the adsorption kinetics data were analyzed by zero-order model, pseudo-first order model and pseudo-second-order model, respectively [60].

The zero-order model:

$$\frac{dQ_t}{dt} \propto k_0 \quad (9)$$

Table I Physical characteristic parameters of IIP and NIIP

parameter	unit	IIP	NIIP
S_{BET}	m^2/g	129.6934	98.8012
V_p	cm^3/g	0.58609	0.292392
d_p	nm	17.2639	11.37749

Where, Q_t (mmol/g) was the amounts of ReO_4^- adsorbed at time t . K_0 was the zero-order rate constant.

By integrating eq. (9), the eq. (10) was obtained.

$$Q_t \propto K_0 t \quad (10)$$

The pseudo-first order model:

$$\frac{dQ_t}{dt} \propto K_1 (Q_e - Q_t) \quad (11)$$

Where, Q_e was the amounts of ReO_4^- adsorbed at equilibrium time (t_e), K_1 was the pseudo-first order rate constant. By integrating eq. (11) at the boundary conditions $Q_t=0$ at $t=0$ and $Q_t=Q_t$ at time t , the eq. (12) was obtained.

$$\ln(Q_e - Q_t) \propto -K_1 t \quad (12)$$

The pseudo-second-order model:

$$\frac{dQ_t}{dt} \propto K_2 (Q_e - Q_t)^2 \quad (13)$$

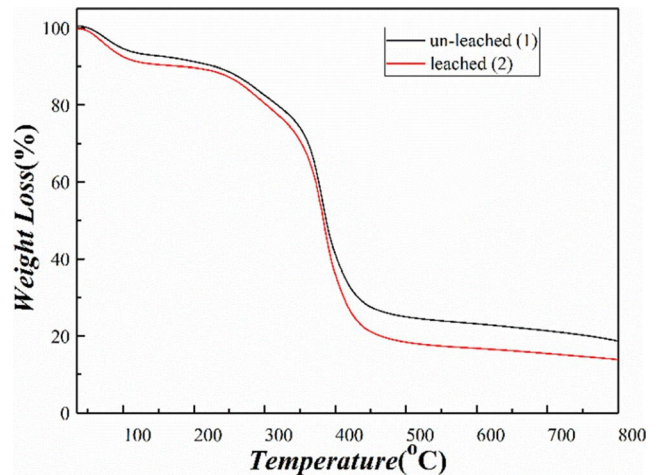


Fig. 5 the TGA curve of IIPs

Table 2 Thermogravimetric analysis

Specimens	First Stage content(%)	Second Stage content(%)	Third Stage content(%)
1	50 °C -131.3 °C, 8.52	201 °C -326 °C, 13.5	326 °C -550 °C, 58.9
2	50 °C -148.5 °C, 7.56	230 °C -338 °C, 13.7	338 °C -550 °C, 53.3

Where, K_2 was the rate constant of pseudo-second-order model. By integrating eq. (13) at the boundary conditions $Q_t=0$ at $t=0$ and $Q_t=Q_e$ at time t , the eq. (14) was obtained.

$$\frac{Q_e}{Q_t} - \frac{1}{K_2 Q_e^2} = \frac{1}{Q_e} + K_2 t \quad (14)$$

Fig. S5 (a) showed regressed results of experimental data. It documented that the zero-order model ($R^2 = 0.9981$, Fig. S5 (a)) was more suitable to express the adsorption kinetics than the pseudo-first-order model ($R^2 = 0.7891$, Fig. S5 (b)) and the pseudo-second-order model ($R^2 = 0.3201$, Fig. S5 (b)), which could be understood that both ReO_4^- and imprinted cavities were sufficient, but the entrance of ReO_4^- into imprinted cavities was slow just like that of the enzymatic reaction process [61]. The reason could be ascribed to the very high steric resistance of IIP matrix which was resulted from high crosslinking degree, and further held back the direction adjusting of ReO_4^- to suit to direction and enter the imprinted cavities.

Adsorption thermodynamics of ReO_4^- -IIP

The relationship between adsorption capacity and the concentration of original solution was shown in Fig. S6. It documented that Q_e increased quickly with increasing of the original concentration of solution till the original concentration reached 1.5 mmol/L. Thereafter, the increase degree of Q_e decreased gradually till the saturated adsorption capacity was arrived at. The variation of Q_e could be ascribed to the transfer among adsorption sites. Because there were different sorts of adsorption sites, i.e. complete imprinted cavities (CIC), imprinting cavities with some defects (ICD) and free active loci (FAL) [62] existed in the network of the IIP, and the adsorption ability of these sites was different. Thus, the adsorption would start at the strongest affinity sites, CIC, first, and terminated at the weakest sites, FAL. At low concentration of ReO_4^- , the adsorption was mainly realized by CIC, because high affinity of CIC to ReO_4^- , the equilibrium constant was large, and Q_e increased with a related high degree. With the increase of concentration, the adsorption gradually transferred to ICD and FAL, because of the lower and lower affinity to ReO_4^- , the increase degree of Q_e decreased gradually.

To investigate the exist of different adsorption sites, Scatchard model [63] was conscripted to evaluate sorts of

adsorption sites and the quantities of CIC in IIP, and the equation was shown in follows [64]:

$$\frac{Q}{C_e} = \frac{Q_m - Q}{K_d} \quad (15)$$

Where, Q_m (mmol/g) stood for the maximum equilibrium adsorption capacities, K_d (mmol/L) was the equilibrium dissociation constant of the binding sites.

The simulation results of Scatchard model were shown in Fig. S7. The two distinct sections of the Scatchard plot suggested that the binding sites in IIP were heterogeneous with respect to the affinity for ReO_4^- . The two linear equations for ReO_4^- -IIP could be expressed as follows:

$$\frac{Q_e}{C_e} = -0.323259 Q_e + 0.07698; \quad R^2 = 0.9902 \quad (16)$$

$$\frac{Q_e}{C_e} = -1.21197 Q_e + 0.16351; \quad R^2 = 0.9210 \quad (17)$$

K_d and Q_m values calculated from the slopes and intercepts of the two linear portions. For higher affinity site, K_d and Q_m were 3.0903 mmol/L and 0.2379 mmol/g. For lower affinity site, K_d and Q_m were 0.8251 mmol/L and 0.1349 mmol/g. Contacting with R^2 of two lines, it could be concluded that more than two sorts of binding sites were existed of in ReO_4^- -IIP because of the presented inferior value of R^2 related to lower affinity site.

To explore the adsorption feature of ReO_4^- -IIP in detail, Langmuir and Freundlich models [65, 66] were conscripted to simulate the experimental data according to divide results of Scatchard model as follows.

Freundlich model:

$$\ln Q_e = \frac{1}{n} \ln C_e + \ln K_F \quad (18)$$

Langmuir model:

$$\frac{C_e}{Q_e} = \frac{C_e}{Q_m} + \frac{K_L}{Q_m} \quad (19)$$

Where, K_L, K_F was adsorption equilibrium constant.

Fig. S8 (a) and (b), respectively, documented the analyzed results. It could be found that Langmuir model was more suitable for describing the isothermal adsorption feature of ReO_4^- -IIP [67], which indicated the adsorption was a mono layer adsorption, and could be understood easily because high crosslinking degree made the multi-layer adsorption took place hardly.

Influence of polymerization temperature (T) on separation performance of ReO_4^- -IIP

The influence of polymerization temperature (T) on separation performance of ReO_4^- -IIP was shown in Fig. S9. It could be seen that with the polymerization temperature (T) increasing, $Q(\text{ReO}_4^-)$, $Q(\text{MnO}_4^-)$ and R increased first and then decreased, and reached the maximum at 35 °C. The polymerization could be initiated hardly at low T , which would result in large quantities of soluble components in the network naturally, and result in the poor completeness of imprinting cavities and the low content of CIC. Simultaneously, due to the removal of the template ions in the late stage, the soluble components would be removed, which would increase the amount of free functional groups (FFG). Because the strong interaction among FFG, the matrix of IIP would collapse, imprinted cavities would deform and even be buried. As a result, the number of efficient adsorption sites (EAS) in IIP would be low, and most of EAS were FAL and dead angle (DA, due to the deformation of imprinted cavities and matrix, some adsorption sites would become difficult for both the ingress and egress of ReO_4^- , which here we called it dead angle, which preferred to adsorb MnO_4^- because of both smaller molecular size and volume), only a few of them were CIC. Because FAL had poor adsorption selectivity for ions and weak interaction with ions, the adsorption of IIP on ions was mainly based on CIC and DA, Q showed a low value naturally. The adsorption force and selectivity for above three sorts of EAS were different, the adsorption force and selectivity of FAL was low, it could adsorb easily, the adsorption force of DA was high, but the selectivity was poorer, while adsorption force and selectivity of CIC were excellent, R was high value relatively. With the increase of T , polymerization and crosslinking reaction increased to complete gradually, the quantities of soluble polymer FFG decreased, the collapse of IIP matrix and the deformation of imprinted cavities would decrease gradually, and CIC increased, while FAL and DA decreased naturally. At this condition, Q and R increased correspondingly. As T continually increase to an unsuitable value, the reaction rate would accelerate, which would result the internal explosion and the destruction of the formed self-assembled structure, FFG increased again. Just as that of in low T , FAL and DA increased, while CIC decreased, Q and R decreased.

Influence of polymerization time (t) on separation performance of ReO_4^- -IIP

The influence of polymerization time (t) on separation performance of ReO_4^- -IIP was shown in Fig. S10. It could be seen that with the polymerization time (t) increased, $Q(\text{ReO}_4^-)$, $Q(\text{MnO}_4^-)$ and R increased first and then decreased. There were chain polymerization and

stepwise polymerization in the preparation process of IIP. In the initial stage of polymerization, the chain reaction (polymerization and crosslinking reaction) was incomplete. There were a large number of soluble polymers in IIP and FFG increased. As soluble polymers were eluted through extraction, imprinted cavities would collapse and deform, EAS decreased, while the relative content of FAL and DA increased. Just as discussed above, Q presented a low value. Because MnO_4^- was mainly adsorbed by DA, while ReO_4^- was mainly adsorbed by CIC, R documented a relatively high value naturally. With the increase of polymerization time, the chain reaction tended to be complete and the crosslinking degree of ReO_4^- -IIP increased, FFG decreased and CIC increased in the ReO_4^- -IIP, while FAL and DA decreased. At this condition, Q increased. Because of the similar structure and smaller size and volume, CIC could also adsorb MnO_4^- with a strong affinity. Added to the affection of equilibrium principal, which would result in a small decrease of R correspondingly. After the polymerization time prolonged unsuitable, the dominant reaction of the polymerization would be gradually transferred to stepwise polymerization, which would increase the amount of FFG in the IIP. The stepwise polymerization was not conducive to the retention of the shape of imprinted cavities, imprinted cavities would deform to DA, and Q and R decreased naturally.

Influence of $n(\text{AA})/n(\text{NVP})$ on separation performance of ReO_4^- -IIP

The influence of $n(\text{AA})/n(\text{NVP})$ on separation performance of ReO_4^- -IIP was shown in Fig. S11. It could be seen that as the $n(\text{AA})/n(\text{NVP})$ increased, $Q(\text{ReO}_4^-)$, $Q(\text{MnO}_4^-)$ and R increased first and then decreased, and reached the maximum at $n(\text{AA})/n(\text{NVP}) = 1.95$. The effect of functional monomer self-assembly was determined by the synergistic effect of two functional monomers. When $n(\text{AA})/n(\text{NVP})$ was small, the synergistic effect of functional monomers was not perfect, functional monomers would self-assembly incompletely and the quantities of FFG increased, which would induce the deform of imprinted cavities, and further result in more quantities of DA, Q and R presented a low value. With the increase of $n(\text{AA})/n(\text{NVP})$, the self-assembly effect would be more complete, the quantities of FFG decreased, which resulted in the increase of CIC, while the decrease of FAL and DA, and further resulted in the increase of Q and R . However, excessive increase of $n(\text{AA})/n(\text{NVP})$ would cause the surplus of AA, and incomplete self-assembly occurred again. FFG increased again, just as that of low $n(\text{AA})/n(\text{NVP})$, Q and R decreased again.

Influence of $n(\text{Vc})/n(\text{NVP})$ on separation performance of ReO_4^- -IIP

The influence of $n(\text{Vc})/n(\text{NVP})$ on separation performance of ReO_4^- -IIP was shown in Fig. S12. It could be seen that as the $n(\text{Vc})/n(\text{NVP})$ increased, $Q(\text{ReO}_4^-)$, $Q(\text{MnO}_4^-)$ and R increased first and then decreased, and reached the maximum at $n(\text{Vc})/n(\text{NVP}) = 0.003$. When $n(\text{Vc})/n(\text{NVP})$ was low, the lower amount of co-initiator Vc in the reaction system resulted in a slower reaction rate of polymerization. Although ReO_4^- -IIP could be formed, the degree of polymerization and crosslinking were both low, there was a large amount of soluble polymer in the network structure. As discussed above, soluble polymers were eluted through extraction, imprinted cavities would collapse and deform, EAS and CIC decreased, while the relative content of FAL and DA increased. Q and R were lower. With the increase of $n(\text{Vc})/n(\text{NVP})$, the number of free radicals in reaction system increased and Vc and H_2O_2 could more completely initiate reaction, which resulted in the degree of polymerization and crosslinking of ReO_4^- -IIP increased and the amount of soluble polymer in the system reduced, FFG decreased and CIC increased, while the amount of FAL and DA decreased correspondingly, Q and R gradually increased naturally. With the excessive increase of $n(\text{Vc})/n(\text{NVP})$, excessive Vc would participate in self-assembly process, and result in a decrease of self-assembly effect, FFG increased again, which would result in the increase of FAL and DA, while the decrease of CIC and EAS correspondingly, Q and R decreased inevitably.

Influence of $n(\text{H}_2\text{O}_2)/n(\text{NVP})$ on separation performance of ReO_4^- -IIP

4

The influence of $n(\text{H}_2\text{O}_2)/n(\text{NVP})$ on separation performance of -IIP was shown in Fig. S13. It could be seen that as the $n(\text{H}_2\text{O}_2)/n(\text{NVP})$ increased, $Q(\text{ReO}_4^-)$, $Q(\text{MnO}_4^-)$, $Q(\text{MnO}_4^-)$ and R increased first and then decreased, and reached the maximum at $n(\text{H}_2\text{O}_2)/n(\text{NVP}) = 0.03$. As the amount of initiator was low, the polymerization rate was slow and the degree of polymerization and crosslinking was low, which resulted in incomplete cavities and large quantities of soluble component and FFG increased, thus CIC and EAS decreased, FAL increased. Q and R showed a low value naturally. With the increase of $n(\text{H}_2\text{O}_2)/n(\text{NVP})$, the rate of polymerization and the degree of polymerization and crosslinking increased, the quantities of FFG decreased. Thus, CIC and EAS increased, FAL and DA decreased, and Q and R increased naturally. When initiator was excessively increased, the reaction rate would accelerate, which would result the internal explosion and the destruction of the formed self-assembled structure. As discussed above, FFG increased again. FAL and DA increased, while CIC decreased, Q and R decreased inevitably.

Influence of $n(\text{NMBA})/n(\text{NVP})$ on separation performance of ReO_4^- -IIP

The influence of $n(\text{NMBA})/n(\text{NVP})$ on separation performance of ReO_4^- -IIP was shown in Fig. S14. It could be seen that as the $n(\text{NMBA})/n(\text{NVP})$ increased, $Q(\text{ReO}_4^-)$, $Q(\text{MnO}_4^-)$ and R increased first and then decreased, and reached the maximum at $n(\text{NMBA})/n(\text{NVP}) = 2.08$. When the amount of NMBA was small, the crosslinking degree of the network was lower, which would result in large amount of soluble polymer and a low rigidity of imprinted cavities, the quantities of FFG increased. Soluble polymer would be eluted and imprinted cavities would be deformed or collapsed during drying and extraction, which lead to a low value of CIC, while a high value FAL and DA, and Q and R showed a low value naturally. With the increase of NMBA, the degree of crosslinking and rigidity of ReO_4^- -IIP increased, the amount of soluble polymer FFG in ReO_4^- -IIP decreased, which resulted in a decrease of FAL and DA, while the increase of CIC, and Q and R increased. However, increasing NMBA excessively would increase the crosslinking degree excessively, FFG increased again, which resulted in the increase of DA, while the decrease of CIC. Therefore, Q and R decreased.

The reusability of ReO_4^- -IIP

The reusability of ReO_4^- -IIP was shown in Fig. 6. It documented that with the repeat time increasing, $Q(\text{ReO}_4^-)$ decreased and then increased at the beginning 7 times, and a minimum presented after repeating for 4 times, after that, $Q(\text{ReO}_4^-)$ decreased and $Q(\text{MnO}_4^-)$ increased gradually. R also gradually decreased with the increase of repeat time. All indexes documented that ReO_4^- -IIP synthesized under the optimal conditions presented a good rigid structure. However, with the repeat time increased, the shape of CIC would deform gradually, and result in a decrease of specific selectivity. In summary, the ReO_4^- -IIP synthesized under the

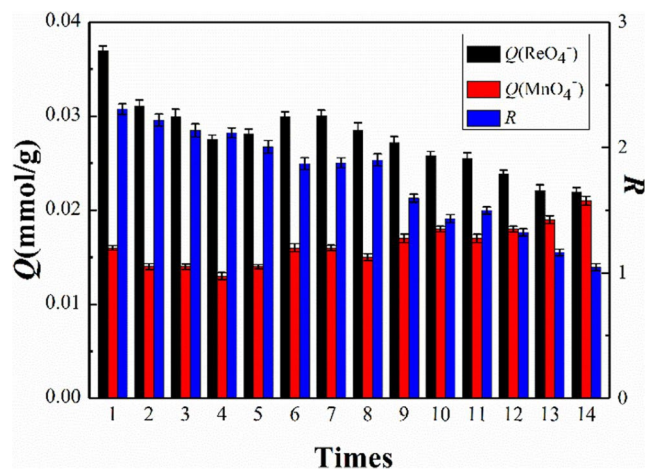


Fig. 6 The reusability of ReO_4^- -IIP

optimal conditions had good reusability, and the effect was best within 7 times.

The specific selectivity of investigation

To verify the specific selectivity of IIP, the adsorption of IIP sample in the binary solution of NH_4ReO_4 and $(\text{NH}_4)_2\text{MoO}_4$, NH_4ReO_4 and NH_4VO_3 , and NH_4ReO_4 and NiCl_2 were selected to conduct study with the same method as that of NH_4ReO_4 and KMnO_4 , and results documented the separation degree were 4.05, 3.98 and 6.00, respectively, which demonstrated ReO_4^- -IIP could separate ReO_4^- with a special selectivity sufficiently.

Conclusions

ReO_4^- -IIP was prepared by solution polymerization using NVP and AA as functional monomers, ReO_4^- as template ion, H_2O_2 -Vc as initiator and NMBA as crosslinker, respectively. The effects of operation conditions on adsorption selectivity were investigated and optimized, and the optimal operation conditions were obtained as follows: the molar ratios of NMBA, AA, H_2O_2 , Vc to NVP were 2.08, 1.95, 0.03 and 0.003, the reaction temperature and time were 35 °C and 24 h, respectively. ReO_4^- -IIP prepared at the optimum conditions documented a good selectivity and reusability. In addition, the adsorption kinetic and the thermodynamic studies presented that the zero-order model and the Langmuir model could better describe the adsorption feature of IIP, and Scatchard model reveals two binding sites for IIP. Finally, the structure and morphology of IIP prepared under the optimal condition was characterized by FTIR, SEM, TEM, BET and TGA respectively, and result showed clear imprinted cavities had been formed in IIP.

Solid phase extraction (SPE), a method commonly used to separate and extract precious metals, is widely used in pharmaceutical, fine chemical, biomedical, food analysis, organic synthesis, environment and other fields thanks to has the advantages of operation simple and fast, low-cost preparation and small dosage of reagent. Although SPE has achieved some results at present, it is still in the development stage. It is believed that in the future, extraction technology with high selectivity, high efficiency and a wide range of applications will have great development prospects.

Acknowledgments This work was supported by Joint fund between Shenyang National Laboratory for Materials Science and State Key Laboratory of Advanced Processing and Recycling of Nonferrous Metals. (18LHZD003;18LHPY004) and Open Project of State Key Laboratory of Nickel and Cobalt Resources Comprehensive Utilization (2019-16).

Compliance with ethical standards

Competing interests The author(s) declare no competing interests.

References

1. Guo JM, He XT, Wang H, Wu XL, Zhao Y (2012) Reviews of metallurgical technology to recovery platinum group metals from secondary resource in China. *Precious Metal* 33:18–23
2. Xin Z, Bai R, Wang D, Cai X, Feng W, Xia M, Yu J (2011) Research development of refractory metal materials used in the field of aerospace. *Rare Metal Mat Eng* 40:1871–1875
3. Liu LF, Wu SS, Chen Y, Lv SL (2016) Oxidation behavior of RE-modified nickel-based superalloy between 950° C and 1150° C in air. *Trans. Nonferrous Met Soc China* 26:1163–1169
4. Li H, He X, Zhao Y (2014) Resources, application and extraction status of rhenium. *Precious Metals* 2:77–81
5. Fleischmann E, Miller MK, Affeldt E, Glatzel U (2015) Quantitative experimental determination of the solid solution hardening potential of rhenium, tungsten and molybdenum in single-crystal nickel-based superalloys. *Acta Mater* 87:350–356
6. Chen X, Tan Z, Wu YF, Liu B, Guo ZJ, Li RB (2017) Recent progress of recovery of scattered metal rhenium from high-temperature alloy scrap. *Mod Chem Ind* 37:60–63
7. Rathkopf C, Mazdab F, Barton I, Barton MD (2017) Grain-scale and deposit-scale heterogeneity of re distribution in molybdenite at the Bagdad porphyry cu-Mo deposit. *Arizona J Geochem Explor* 178:45–54
8. Abdollahi H, Noaparast M, Shafaei SZ, Manafi Z (2015) Acidic leaching with chlorate as oxidizing agent to extract Mo and re from molybdenite flotation concentrate in a copper plant. *Sep Sci Technol* 50:2396–2404
9. Fang DW, Song ZR, Zhang SC, Li J, Zang SL (2017) Solvent extraction of rhenium(VII) from aqueous solution assisted by hydrophobic ionic liquid. *J Chem Eng Data* 62:1094–1098
10. Zang SL, Zhao GS, Zhao HM, Li J, Fang DW (2016) Thermodynamics study of rhenium solvent extraction process from sulfuric acid medium. *J Chem Eng Data* 61:1592–1596
11. Srivastava RR, Kim MS, Lee JC (2016) A novel aqueous processing of the reverted turbine-blade Superalloy for rhenium recovery. *Ind Eng Chem Res* 55:8191–8199
12. Sadrezhaad SK, Alamdari EK (2001) Thermodynamics of extraction of ReO_4^- from aqueous sulfuric acid media with tri-n-butyl phosphate dissolved in kerosene. *Metallurgical & Materials Transactions A* 32:5–10
13. Ansari S, Karimi M (2017) Novel developments and trends of analytical methods for drug analysis in biological and environmental samples by molecularly imprinted polymers. *Trac-Trends Anal Chem* 89:146–162
14. Zhang W, Yun M, Yu Z, Dan C, Xiao L (2019) A novel cu (II) ion-imprinted alginate-chitosan complex adsorbent for selective separation of cu (II) from aqueous solution. *Polym Bull* 76:1861–1876
15. Min L, Feng C, Li M, Zeng Q, Qiang G (2015) Synthesis and application of a surface-grafted in (III) ion-imprinted polymer for selective separation and pre-concentration of indium (III) ion from aqueous solution. *Hydrometallurgy* 154:63–71
16. Zhu F, Li L, Xing J (2017) Selective adsorption behavior of cd (II) ion imprinted polymers synthesized by microwave-assisted inverse emulsion polymerization: adsorption performance and mechanism. *J Hazard Mater* 321:103–110
17. Ebrahimzadeh H, Asgharinezhad AA, Jalilian N, Panjali Z (2015) A simple and fast method based on new magnetic ion imprinted

- polymer nanoparticles for the selective extraction of Ni(II) ions in different food samples. *RSC Adv* 5:45510–45519
18. Lu J, Wu Y, Lin X, Gao J, Dong H, Chen L, Qin Y, Wang L, Yan Y (2018) Anti-fouling and thermosensitive ion-imprinted nanocomposite membranes based on graphene oxide and silicon dioxide for selectively separating europium ions. *J Hazard Mater* 353:244–253
 19. Zeng J, Lv C, Liu G, Zhang Z, Dong Z, Liu J, Wang Y (2019) A novel ion-imprinted membrane induced by amphiphilic block copolymer for selective separation of Pt (IV) from aqueous solutions. *J Membr Sci* 572:428–441
 20. Cui J, Zhou Z, Xie A, Liu S, Wang Q, Wu Y, Yan Y, Li C (2019) Facile synthesis of degradable CA/CS imprinted membrane by hydrolysis polymerization for effective separation and recovery of Li⁺. *Carbohydr Polym* 205:492–499
 21. Gui R, Jin H, Guo H, Wang Z (2018) Recent advances and future prospects in molecularly imprinted polymers-based electrochemical biosensors. *Biosens Bioelectron* 100:56–70
 22. Zhu X, Zeng Y, Zhang Z, Yang Y, Zhai Y, Wang H, Liu L, Hu J, Li L (2018) A new composite of graphene and molecularly imprinted polymer based on ionic liquids as functional monomer and cross-linker for electrochemical sensing 6-benzylaminopurine. *Biosens Bioelectron* 108:38–45
 23. Bagheri H, Shirzadmehr A, Rezaei M, Khoshshafar H (2018) Determination of tramadol in pharmaceutical products and biological samples using a new nanocomposite carbon paste sensor based on decorated nanographene/tramadol-imprinted polymer nanoparticles/ionic liquid. *Ionics* 24(3):833–843
 24. Ahmed MA, Abdelbar NM, Mohamed AA (2018) Molecular imprinted chitosanTiO₂ nanocomposite for the selective removal of rose Bengal from wastewater. *Int J Biol Macromol* 107:1046–1053
 25. de León-Martínez LD, Rodríguez-Aguilar M, Ocampo-Pérez R, Gutiérrez-Hernández JM, Díaz-Barriga F, Batres-Esquivel L, Flores-Ramírez R (2018) Synthesis and Evaluation of a Molecularly Imprinted Polymer for the Determination of Metronidazole in Water Samples 100(3):1–7
 26. Lins SS, Virgens CF, dos Santos WNL, Estevam IHS, Brandão GC (2019) On-line solid phase extraction system using an ion imprinted polymer based on dithizone chelating for selective preconcentration and determination of mercury (II) in natural waters by CV AFS. *Microchem J* 150:104075
 27. Fang L, Min X, Kang R, Yu HY, Pavlostathis SG, Luo XB (2018) Development of an anion imprinted polymer for high and selective removal of arsenite from wastewater. *Sci Total Environ* 639:110–117
 28. Zarezade V, Behbahani M, Omid F, Abandansari HS, Hesam G (2016) A new magnetic tailor made polymer for separation and trace determination of cadmium ions by flame atomic absorption spectrophotometry. *RSC Adv* 6(105):103499–103507
 29. Kakavandi MG, Behbahani M, Omid F, Hesam G (2017) Application of ultrasonic assisted-dispersive solid phase extraction based on ion-imprinted polymer nanoparticles for preconcentration and trace determination of lead ions in food and water samples. *Food Anal Methods* 10(7):2454–2466
 30. Behbahani M, Salarian M, Bagheri A, Tabani H, Omid F, Fakhari A (2014) Synthesis, characterization and analytical application of Zn(II)-imprinted polymer as an efficient solid-phase extraction technique for trace determination of zinc ions in food samples. *Journal of Food Composition & Analysis* 34(1):81–89
 31. Behbahani M, Barati M, Bojdi MK, Pourali AR, Bagheri A, Tapeh NA (2013) A nanosized cadmium(II)-imprinted polymer for use in selective trace determination of cadmium in complex matrices. *Mikrochimica Acta* 180(11):1117–1125
 32. Ebrahimzadeh H, Behbahani M, Yamini Y, Adlnasab L, Asgharinezhad AA (2013) Optimization of cu(II)-ion imprinted nanoparticles for trace monitoring of copper in water and fish samples using a box–Behnken design. *Reactive & Functional Polymers* 73(1):23–29
 33. Ji WH, Sun RH, Geng YL, Liu W, Wang X (2018) Rapid, low temperature synthesis of molecularly imprinted covalent organic frameworks for the highly selective extraction of cyano pyrethroids from plant samples. *Anal Chim Acta* 1001:179–188
 34. Parvizi S, Behbahani M, Esrafil A (2018) Preconcentration and ultra-trace determination of hexavalent chromium ions using tailor-made polymer nanoparticles coupled with graphite furnace atomic absorption spectrometry: ultrasonic assisted-dispersive solid-phase extraction. *New J Chem* 42(12):10357–10365
 35. Behbahani M, Omid F, Kakavandi MG, Hesam G (2017) Selective and sensitive determination of silver ions at trace levels based on ultrasonic-assisted dispersive solid-phase extraction using ion-imprinted polymer nanoparticles. *Appl Organomet Chem* 31(11):3758
 36. Ghorbani-Kalhor E, Behbahani M, Abolhasani J (2015) Application of ion-imprinted polymer nanoparticles for selective trace determination of palladium ions in food and environmental samples with the aid of experimental design methodology[J]. *Food Anal Methods* 8(7):1746–1757
 37. Behbahani M, Hassanlou PG, Amini MM, Moazami HR, Abandansari HS, Bagheri A, Zadeh SH (2015) Selective solid-phase extraction and trace monitoring of Lead ions in food and water samples using new Lead-imprinted polymer nanoparticles. *Food Anal Methods* 5(8):558–568
 38. Ghorbani-Kalhor E, Behbahani M, Abolhasani J, Hosseinzadeh KR (2015) Synthesis and characterization of modified multiwall carbon nanotubes with poly (N-Phenylethanolamine) and their application for removal and trace detection of Lead ions in food and environmental samples[J]. *Food Anal Methods* 8(5):1326–1334
 39. Bitas D, Samanidou V (2018) Molecularly imprinted polymers as extracting media for the chromatographic determination of antibiotics in milk. *Molecules* 23(2):316
 40. Paul PK, Treetong A, Suedee R (2017) Biomimetic insulin-imprinted polymer nanoparticles as a potential oral drug delivery system. *Acta Pharma* 67(2):149–168
 41. Gao B, Du J, Zhang Y (2013) Preparation of arsenate anion surface-imprinted material IIP-PDMC/SiO₂ and study on its ion recognition property. *Ind Eng Chem Res* 52:7651–7659
 42. Zhou Z, Kong D, Zhu H (2018) Preparation and adsorption characteristics of an ion-imprinted polymer for fast removal of Ni(II) ions from aqueous solution. *J Hazard Mater* 341:355–364
 43. Alizadeh T, Atayi K (2018) Synthesis of hydrogen phosphate anion-imprinted polymer via emulsion polymerization and its use as the recognition element of graphene/graphite paste potentiometric electrode. *Materials Chemistry & Physics* 209:180–187
 44. Zhai Y, Yang D, Chang X, Liu Y, He Q (2015) Selective enrichment of trace copper(II) from biological and natural water samples by SPE using ion-imprinted polymer. *J Sep Sci* 31:1195–1200
 45. Huang K, Li B, Zhou F, Mei S, Zhou Y, Jing T (2016) Selective solid-phase extraction of lead ions in water samples using three-dimensional ion-imprinted polymers. *Anal Chem* 88:6820–6826
 46. Kong D, Wang N, Ning Q, Qi W, Zhuo W, Zhou Z, Ren Z (2017) Facile preparation of ion-imprinted chitosan microspheres enwrapping Fe₃O₄ and graphene oxide by inverse suspension crosslinking for highly selective removal of copper (II). *ACS Sustain Chem Eng* 5:7401–7409
 47. Daoud AM, Zhao Y, Elkak A, Falcimaigne-Cordin A, Haupt K (2017) Enzyme-initiated free-radical polymerization of molecularly imprinted polymer Nanogels on a solid phase with an immobilized radical source. *Angew Chem* 129:3387–3391
 48. Zhou T, Ding L, Che G, Jiang W, Sang L (2019) Recent advances and trends of molecularly imprinted polymers for specific recognition in aqueous matrix: preparation and application in sample pretreatment. *Trac-Trends Anal Chem* 114:11–28

49. Zhao Y, Chen Z, Li J, Liu Z, Liu D, Li Z (2017) Preparative separation and purification of flavonoids from *Lamiophlomis rotata* (Benth) Kudo Pigm Resin Technol 46:496-506
50. Zhao Y, Chen Z, Liu D, Long J, Di D (2017) Separation of flavonoids in the leaves of *Sophora japonica* by macroporous adsorption resin mixed-bed technology. Pigm Resin Technol 46:235-243
51. Deng GC, Teng HH, Zhang YY, Zhao LY, Wei M, Wang YJ, Zang SL (2006) Spectrophotometric determination of trace rhenium in molybdenum samples using the system of ReO₄-ethyl violet-polyvinyl alcohol. Metal Anal 26:27-29
52. Fang P, Xia W, Zhou Y, Ai Z, Yin W, Xia M, Yue Q (2020) Ion-imprinted mesoporous silica/magnetic graphene oxide composites functionalized with Schiff-base for selective Cu(II) capture and simultaneously being transformed as a robust heterogeneous catalyst. Chem Eng J 6:10
53. Samah NA, Rosli NAM, Manap AHA, Aziz YFA, Yusoff MM (2020) Synthesis & characterization of ion imprinted polymer for arsenic removal from water: a value addition to the groundwater resources. Chem Eng J 394:124900
54. Wang Y, Zhou J, Zhang B, Tian L, Ali Z, Zhang Q (2017) Fabrication and characterization of glutathione-imprinted polymers on fibrous SiO₂ microspheres with high specific surface. Chem Eng J 327:932-940
55. Tanodekaew S, Prasitsilp M, Swadison S, Thavornnyutikarn B, Pothsree T, Pateepasen R (2004) Preparation of acrylic grafted chitin for wound dressing application. Biomaterials 25(7):1453-1460
56. Thurmer MB, Diehl CE, Brum FJ, Santos LA (2014) Preparation and characterization of hydrogels with potential for use as biomaterials. Materials Research-ibero-american Journal of Materials: 109-113
57. Lin C, Lee C, Chiu W (2005) Preparation and properties of poly(acrylic acid) oligomer stabilized superparamagnetic ferrofluid. J Colloid Interface Sci 291(2):411-420
58. Moharram MA, Allam MA (2007) Study of the interaction of poly(acrylic acid) and poly(acrylic acid-poly acrylamide) complex with bone powders and hydroxyapatite by using TGA and DSC. J Appl Polym Sci 105(6):3220-3227
59. Han HL (2019) Study on Thermolysis of ammonium Perrhenate and application on silver catalyst. Journal of Qilu University of Technology 33(03):35-38
60. Nakhjiri MT, Marandi GB, Kurdtabar M (2018) Poly(AA-co-VPA) hydrogel cross-linked with N -maleyl chitosan as dye adsorbent: isotherms, kinetics and thermodynamic investigation. Int J Biol Macromol 117:152-166
61. Blackmond DG (2005) Reaction progress kinetic analysis: a powerful methodology for mechanistic studies of complex catalytic reactions. Angew Chem-Int Edit 44:4302-4320
62. Valderrama C, Cortina J, Farran A, Gamisans X, de Las HF (2008) Kinetic study of acid red "dye" removal by activated carbon and hyper-cross-linked polymeric sorbents macronet Hypersol MN200 and MN300. React Funct Polym 68:718-731
63. Mergola L, Scorrano S, Bloise E, Di Bello MP, Catalano M, Vasapollo G, Del Sole R (2016) Novel polymeric sorbents based on imprinted Hg (II)-diphenylcarbazone complexes for mercury removal from drinking water. Polym J 48:73-79
64. Matsui J, Miyoshi Y, Doblhoff-Dier O, Takeuchi T (1995) A molecularly imprinted synthetic polymer receptor selective for atrazine. Anal Chem 67:4404-4408
65. Niu Y, Qu R, Chen H, Mu L, Liu X, Wang T, Zhang Y, Sun C (2014) Synthesis of silica gel supported salicylaldehyde modified PAMAM dendrimers for the effective removal of Hg (II) from aqueous solution. J Hazard Mater 278:267-278
66. Liu Y, Xu L, Liu J, Liu X, Chen C, Li G, Meng Y (2016) Graphene oxides cross-linked with hyperbranched polyethylenimines: preparation, characterization and their potential as recyclable and highly efficient adsorption materials for lead (II) ions. Chem Eng J 285: 698-708
67. Guo B, Deng F, Zhao Y, Luo X, Luo S, Au C (2014) Magnetic ion-imprinted and-SH functionalized polymer for selective removal of Pb (II) from aqueous samples. Appl Surf Sci 292:438-446